Wavefront reconstruction algorithm for wavefront sensing based on binary aberration modes*

Boqing Pang(庞博清)[1,2,3], Shuai Wang(王帅)[1,3], Tao Cheng(程涛)[1,2,3], Qingfeng Kong(孔庆峰)[1,2,3,4], Lianghua Wen(文良华)[1,2,3,5], and Ping Yang(杨平)[1,3,†]

[1] *Key Laboratory on Adaptive Optics, Chinese Academy of Sciences, Chengdu* 610209, *China*
[2] *University of Chinese Academy of Sciences, Beijing* 100049, *China*
[3] *The Institute of Optics and Electronics, Chinese Academy of Sciences, Chengdu* 610209, *China*
[4] *School of Optoelectronic information, University of Electronic Science and Technology of China, Chengdu* 610209, *China*
[5] *School of Physics and Electronic Engineering, Yibin University, Yibin* 644000, *China*

(Received 26 October 2016; revised manuscript received 10 January 2017; published online 30 March 2017)

We propose a new algorithm for wavefront sensing based on binary intensity modulation. The algorithm is based on the fact that a wavefront can be expended with a series of orthogonal and binary functions, the Walsh series. We use a spatial light modulator (SLM) to produce different binary-intensity-modulation patterns which are the simple linear transformation of the Walsh series. The optical fields under different binary-intensity-modulation patterns are detected with a photodiode. The relationships between the incident wavefront modulated with the patterns and their optical fields are built to determinate the coefficients of the Walsh series. More detailed and strict relationship equations are established with the algorithm by adding new modulation patterns according to the properties of the Walsh functions. An exact value can be acquired by solving the equations. Finally, with the help of phase unwrapping and smoothing, the wavefront can be reconstructed. The advantage of the algorithm is providing an analytical solution for the coefficients of the Walsh series to reconstruct the wavefront. The simulation experiments are presented and the effectiveness of the algorithm is demonstrated.

Keywords: wavefront sensing, binary aberration modes, Walsh functions, single detector

PACS: 42.25.–p, 42.15.Fr, 42.30.Kq, 42.30.Wb **DOI:** 10.1088/1674-1056/26/5/054204

1. Introduction

Wavefront sensing has been an indispensible part for adaptive optics (AO) systems. A typical adaptive optics system must have a way to sense the wavefront with enough spatial resolution and time resolution to apply a real-time correction.[1] The requirements of wavefront sensing in an adaptive optics system have a great difference from those of phase or figure determination in optical testing.[2] The wavefront sensing frequency can be on the order of hundreds of hertz. Meanwhile, with the wide applications of adaptive optics in a wide range from astronomical telescopes to microscopy, new challenges arise to meet the stringent requirements in applications, such as ground-based telescopes observing weak objects through the atmosphere.[3,4] Higher requirements on speed and sensitivity for wavefront sensing sensors are urgently necessary. However, most of the conventional wavefront sensing techniques use array detectors to acquire signals, such as Shack–Hartmann wavefront sensing,[5] curvature sensing,[6] and phase retrieval.[7] Two-dimensional detectors have significant limitations, especially in speed and sensitivity. They are also very expensive and hard to manufacture. In many cases, the array detectors working in some special conditions, such as weak light or high noise, often have low signal-to-noise ratios and cannot reconstruct the wavefront with enough accuracy. So another wavefront sensing approach measuring the wavefront with a single detector comes into consideration.[8,9] Compared with array detectors, single detectors ordinarily have higher performance and lower price. Due to the structure character, designs with single detectors can focus the light of the entire aperture and realize measurement without the light beam splitting and dividing. For this reason, the design of wavefront sensing with a single detector is likely to acquire a high signal-to-noise ratio under the condition of weak light. Besides, the signals detected with a single detector are one-dimensional, which means that the quantity of data is rather small. It provides a relative lower requirement on transmission and computing. Obviously, it is a potential heuristic direction sensing wavefront with a single detector.

There are two known papers realizing wavefront sensing using a single detector through the measurements of binary aberration modes.[10,11] The most outstanding contribution of them is providing a new way of wavefront sensing with a single detector. It can realize wavefront sensing with enough spatial resolution and speed which opens a great potentiality in adaptive optics system. Both of them expend the incident wavefront with a series of orthogonal and binary functions, the mode-field-Walsh (MOW) functions. The difference be-

*Project supported by the National Innovation Fund of Chinese Academy of Sciences (Grant No. CXJJ-16M208), the Preeminent Youth Fund of Sichuan Province, China (Grant No. 2012JQ0012), and the Outstanding Youth Science Fund of Chinese Academy of Sciences.

†Corresponding author. E-mail: pingyang2516@163.com

© 2017 Chinese Physical Society and IOP Publishing Ltd

tween them lies in that Feiling Wang manipulates the wavefront with binary phase patterns and Shuai Wang uses binary intensity patterns. A relationship equation between the coefficients of the MOW functions and their optical fields has been built. However, based on the iterative algorithm[3] or optimization strategy,[11] they can only obtain approximations of the coefficients by solving the equations. The low speed of the algorithms and the uncertain accuracy of the approximations limit the speed of the single detector as well as the method. So an algorithm that can provide exact coefficients with high speed is necessary and becomes the key point for the wavefront sensing method working well in real-time adaptive optics systems.

In this paper, we present a new algorithm which provides an analytic solution for the coefficients of the MOW functions. New selected modulation patterns derived from the linear transformation of the MOW functions are replenished for the algorithm. According to the modulation patterns, new relationships between the supplementary modulation patterns and their intensity signals (the light intensity within the pin hole) are built to determine an analytical solution for the coefficients of the MOW functions. A discrete wrapping wavefront whose phase is in the range of $[-\pi, \pi]$ can be acquired with the coefficients. Phase unwrapping and smoothing methods are applied to transform the discrete wrapping wavefront into a continuous wavefront. This provides a possibility for the wavefront sensing method used in real-time adaptive optics systems.

2. Mathematical foundation

2.1. Walsh functions

In order to realize wavefront sensing through intensity modulation, it is necessary to establish the connection between intensity and phase. It should be noted that no light is a special situation in intensity modulation which means that the amplitude and phase of light disappear at the same time. Meanwhile, when the amplitude of the modulated light is not zero, the phase of the modulated light keeps the same as that of the incident light. So the intensity modulation produces two kinds of special statements, "light on" meaning that the phase is chosen and "light off" meaning the phase is ignored.

The set of Walsh functions is a series of complete and orthogonal binary functions that take on two values, -1 and $+1$. The MOW functions are derived from the two-dimensional Walsh functions in the polar coordinates. The Walsh functions are formed by dividing the azimuth angle and the radius. The division is used to produce an orthogonal and complete series in the circular aperture. Figure 1 depicts a few two-dimensional Walsh functions in the polar coordinates. The intensity modulation patterns can be derived from the Walsh series by simple linear transformation.[11]

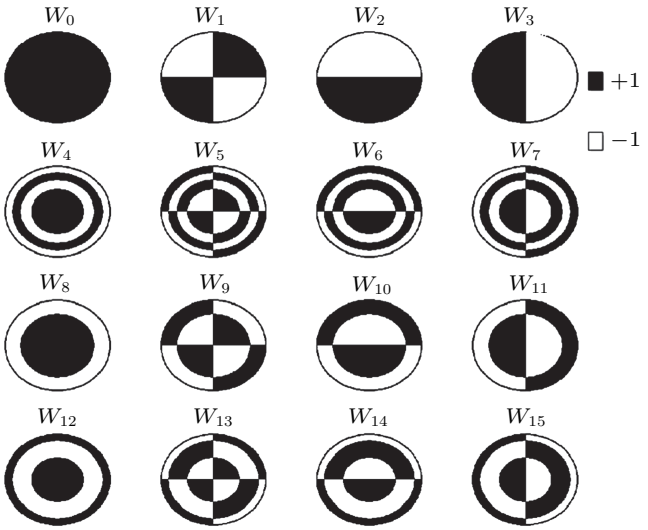


Fig. 1. The two-dimensional Walsh functions in polar coordinates, $W_q = W_n(r)W_m(\theta)$, $n = 0,1,2,3$, $m = 0,1,2,3$, $q = 4n+m$.

The Walsh functions have an important property

$$W_m \cdot W_n = W_{m\oplus n}, \tag{1}$$

where operator $\oplus$ denotes binary addition.

2.2. Principle of wavefront sensing

The optical arrangement of the wavefront sensing is shown in Fig. 2. An intensity SLM modulator is used to modulate the incident wavefront. A lens focuses the modulated light beam into the photodiode. The pinhole works as the binary-aberration-mode filter. The photodiode detects the intensity signal.

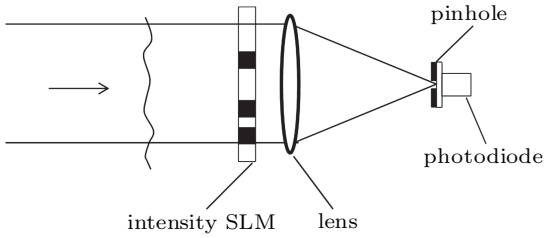


Fig. 2. Optical arrangement for wavefront sensing using the proposed method.

According to the Fourier diffraction theory, the signal measured at the ideal focal point by the photodiode is given by[8]

$$\mathrm{I} = D_0 \left| \iint\limits_A E(x,y)\,\mathrm{d}x\mathrm{d}y \right|^2 = D_0 \left| \iint\limits_A E_0 \mathrm{e}^{\mathrm{i}\varphi}\,\mathrm{d}x\mathrm{d}y \right|^2, \tag{2}$$

where D_0 is a constant, $E(x,y)$ is the optical field of the incident light, and E_0 and φ are the amplitude and phase of the incident light. The intensity signal stays the same when the phase of the incident wavefront is inverted or adds a fixed value φ_0 as

$$\left| \iint\limits_A E_0 \mathrm{e}^{\mathrm{i}(\pm\varphi+\varphi_0)}\,\mathrm{d}x\mathrm{d}y \right|^2 = \left| \iint\limits_A E_0 \mathrm{e}^{\mathrm{i}\varphi}\,\mathrm{d}x\mathrm{d}y \right|^2. \tag{3}$$

As shown in Eq. (3), the phase of the reconstructed wavefront could be $\pm\varphi+\varphi_0$ used rather than φ. The value of φ_0 has no contribution to the wavefront aberrations. So in order to obtain the solution, we can set the value of φ_0 depending on our needs.

We expand the aberration function of the incident wavefront with the MOW functions in the following form:

$$e^{i\varphi}=\cos\varphi+i\sin\varphi=\sum_{l=0}^{N}a_lW_l+i\sum_{l=0}^{N}b_lW_l=\sum_{l=0}^{N}B_lW_l, \quad (4)$$

where l can be any integer from 0 to N, a_l, and b_l are the expansion MOW-function coefficients of $\cos\varphi$ and $\sin\varphi$, respectively, and B_l is the l-th expansion coefficient of the incident wavefront phase,

$$B_l=a_l+ib_l. \quad (5)$$

We expand the real and the imaginary parts of the incident light field respectively. It differs from the expansion of the wavefront phase directly which would bring a coupling on the coefficients of the MOW functions.[10,11] The coupling of the coefficients makes it difficult to acquire an analytical solution. In contrast, the expansion form described in the paper can avoid the coupling.

In order to acquire the coefficients of the MOW functions, we need to build connections between the modulation patterns and the MOW functions. The intensity SLM modulator can only influence the amplitude of the incident light directly. As discussed above, the intensity modulation produces two kinds of special statements, light on and light off. So a set of relationships between the binary-intensity-modulation patterns and the MOW functions can be built by a simple linear transformation[11]

$$T_k=\frac{1+W_k}{2}, \quad (6)$$

where the index k can be any integer from 0 to N, W_k is the k-th MOW function, and T_k is the k-th binary-intensity-modulation pattern, which has only two values, 0 and 1, that exactly correspond to light off and light on. When the incident wavefront is modulated with T_k, the phase of specific parts can be selected and detected.

The wavefront modulated with the binary-intensity-modulation patterns can be described as

$$\begin{aligned}T_kE(x,y) &= E_0\frac{1+W_k}{2}\sum_{l=0}^{N}B_lW_l\\ &= \frac{E_0}{2}\left[\sum_{l=0}^{N}B_lW_l+W_k\sum_{l=0}^{N}B_lW_l\right]. \end{aligned}\quad (7)$$

The corresponding intensity signal measured by the photodiode is given by [10]

$$I_k=D\frac{E_0^2}{4}\left|B_0+B_k\right|^2, \quad (8)$$

where D is a constant, and B_0 and B_k are the coefficients of the MOW functions.

As discussed above, the phase of the reconstructed wavefront is $\pm\varphi+\varphi_0$ rather than φ. The value of φ_0 has no contribution to the wavefront aberrations. According to Eq. (4), we have

$$e^{i(\varphi+\varphi_0)}=e^{i\varphi_0}\sum_{l=0}^{N}B_lW_l=\sum_{l=0}^{N}(e^{i\varphi_0}B_l)W_l=\sum_{l=0}^{N}B'_lW_l, \quad (9)$$

with

$$B'_l=e^{i\varphi_0}B_l, \quad (10)$$

where B'_l is the l-th expansion MOW-function coefficient of $e^{-i(\varphi+\varphi_0)}$. When $l=0$, we can set B'_0 to be a real number by setting the value of φ_0. According to Eq. (8), the intensity signal measured by the photodiode can be rewritten as

$$\begin{aligned}I_k &= D\frac{E_0^2}{4}\left|B_0+B_k\right|^2=D\frac{E_0^2}{4}\left|e^{-i\varphi_0}(B'_0+B'_k)\right|^2\\ &= D\frac{E_0^2}{4}\left|B'_0+B'_k\right|^2. \end{aligned}\quad (11)$$

When $k=0$, we obtain

$$B'_0=\frac{\sqrt{I_0}}{E_0\sqrt{D}}. \quad (12)$$

Because B'_k are imaginary numbers (k is any integer from 1 to N), we need to build $2N$ equations for the calculation of the coefficients of the MOW functions at least. So we add binary-intensity-modulation patterns

$$T'_k=\frac{1-W_k}{2}, \quad (13)$$

and the corresponding intensity signal I'_k can be written as

$$I'_k=D\frac{E_0^2}{4}\left|B'_0-B'_k\right|^2. \quad (14)$$

By solving Eqs. (11) and (14), we obtain

$$\begin{aligned}&B'_0=a'_0=\frac{\sqrt{I_0}}{E_0\sqrt{D}},\quad B'_k=a'_k+ib'_k,\\ &a'_k=\frac{(I_k-I'_k)}{a'_0DE_0^2},\quad b'_k=\pm\sqrt{\frac{2(I_k+I'_k)}{DE_0^2}-a'^2_0-a'^2_k}, \end{aligned}\quad (15)$$

where

$$a'_k=e^{i\varphi_0}a_k,\quad b'_k=e^{i\varphi_0}b_k, \quad (16)$$

and k can be any integer from 1 to N. We cannot ascertain the sign of b'_k because both equations (11) and (14) are nonlinear equations whose solution is not unique. So we can assume that the sign of b'_k is positive. The value of B'_l can be given as

$$B'_1=a'_1+ib'_1,\quad a'_1=\frac{I_1-I'_1}{a'_0DE_0^2},$$

$$b'_1 = \sqrt{\frac{2(I_1 + I'_1)}{DE_0^2} - a'^2_0 - a'^2_1}. \tag{17}$$

When k is larger than 1, the sign of b'_k is still unknown. We need more conditions to ascertain the sign of b'_k. So we add new binary-intensity-modulation patterns $T_{1,2n}$ and $T_{1',2n}$ to solve it.

We choose the Hadamard order to produce the MOW functions in the wavefront sensing method. According to Eq. (1), we can obtain

$$W_{2n+1} = W_1 \cdot W_{2n}. \tag{18}$$

So we produce new binary-intensity-modulation patterns $T_{1,2n}$ and $T_{1',2n}$, which can be described as

$$\begin{aligned} T_{1,2n} &= \frac{1+W_1}{2}\frac{1+W_{2n}}{2} = \frac{1+W_1+W_{2n}+W_{2n+1}}{4}, \\ T_{1',2n} &= \frac{1-W_1}{2}\frac{1+W_{2n}}{2} \\ &= \frac{1-W_1+W_{2n}-W_{2n+1}}{4}, \quad n = 2k, \end{aligned} \tag{19}$$

where the index n can be any integer from 1 to $(N-2)/2$. Accordingly, the intensity signal detected with the photodiode is

$$\begin{aligned} I_{1,2n} &= \frac{DE_0^2}{16}|B'_0 + B'_1 + B'_{2n} + B'_{2n+1}|^2, \\ I_{1',2n} &= \frac{DE_0^2}{16}|B'_0 - B'_1 + B'_{2n} - B'_{2n+1}|^2. \end{aligned} \tag{20}$$

In Eq. (20), only the signs of the imaginary parts of B'_{2n} and B'_{2n+1} are unknown. The values of $I_{1,2n}$ and $I_{1',2n}$ have four different possibilities. Next by comparing the intensity signal with the possible value, we can determine the signs of the imaginary parts of B'_{2n} and B'_{2n+1}.

By now, the coefficients B'_l of the MOW functions can be determined. According to Eq. (9), we can obtain the value of $e^{i(\varphi+\varphi_0)}$. The wavefront phase can be expressed as

$$\varphi = i^{-1}\ln(e^{i(\varphi+\varphi_0)}) = i^{-1}\ln\left(\sum_{l=0}^{N} B'_l W_l\right). \tag{21}$$

3. Phase unwrapping of wavefront

It should be noticed that the value of the wrapped wavefront phase is limited in the range of $[-\pi, \pi]$, which cannot express the true wavefront phase. The phase unwrapping is unavoidable in the reconstruction process of the wavefront phase. The 2π discontinuity of the wrapped wavefront phase appears when an extreme value, $+\pi$ or $-\pi$, is reached and the phase jumps to the other end of the interval. Thus a phase unwrapping method is required for reconstructing the true wavefront. The wrapped wavefront phase can be expressed as

$$\phi = (\varphi + \varphi_0) - 2n\pi, \tag{22}$$

where ϕ is the wrapped phase, $\varphi + \varphi_0$ is the phase of the incident wavefront phase, and n is an integer. So the wavefront phase unwrapping can be done by adding or subtracting multiples of 2π. The process can begin at an arbitrary point of the wavefront phase.

In order to recover the wavefront, the sampling rate should satisfy the Nyquist sampling theory. So phase unwrapping techniques should start from the fact that the phase differences of the neighboring pixels are less than π.[12] And the unwrapping operation is relatively easy to implement when the sampling rate is higher. The unwrapped relative phase can be written as

$$\begin{aligned} &\varphi(n,m) + \varphi_0 \\ &= \begin{cases} \phi(n,m), & |\phi(n,m) - \phi(n',m')| < \pi, \\ \phi(n,m) - 2\pi, & \phi(n,m) - \phi(n',m') > \pi, \\ \phi(n,m) + 2\pi, & \phi(n,m) - \phi(n',m') < -\pi, \end{cases} \end{aligned} \tag{23}$$

where $\varphi(n,m)$ is the unwrapped wavefront, φ_0 is a constant, and $\phi(n,m)$ is the wrapped wavefront phase. $\phi(n,m)$ and $\phi(n',m')$ are the wavefront phases of neighboring pixels. We can unwrap the wavefront by adding or subtracting multiples of 2π according to Eq. (23). Because the incident wavefront is expanded with the MOW functions, the unwrapped wavefront is still a discrete one. The aberration modes are different from the common wavefront phase form. So we make a linear transformation from the MOW functions to Zernike polynomials to acquire a continuous wavefront.[13]

4. Numerical simulation

We produce the incident wavefront with the first 35 Zernike polynomials depending on the power spectrum of the Kolmogorov model for atmospheric turbulence.[14] Figure 3(a) shows the synthesized incident wavefront. Then we produce the binary-intensity-modulation patterns from the first 256 MOW functions and use the patterns to modulate the wavefront. Next we calculate the intensity signal according to Eq. (2). The signals are detected with the single photodiode and are proportional to the incident light power. We compute the coefficients of the MOW functions by the intensity signal. According to Eq. (4), we can acquire the unwrapped wavefront as shown in Fig. 3(b). It is obvious that the reconstructed wavefront phase is wrapped into the range of $[-\pi, \pi]$. It has large differences with the incident wavefront. Then we unwrap the reconstructed wavefront with Eq. (23). Figure 3(c) gives the unwrapped wavefront. We can see that the unwrapped wavefront is similar to the incident wavefront but discrete. It should be noticed that the common wavefront form of light is continuous. Meanwhile, an extra residual wavefront is produced when the continuous incident wavefront is reconstructed with a finite number of discrete functions. It

can be seen from Fig. 3(d) that the PV and RMS of the residual wavefront between the unwrapped wavefront and the incident wavefront are still large. Then we transform the discrete wavefront described with the MOW functions into a continuous wavefront with Zernike polynomials.[11] The continuous wavefront expressed with the Zernike polynomials is shown in Fig. 3(e). The PV and RMS of the residual wavefront become much smaller.

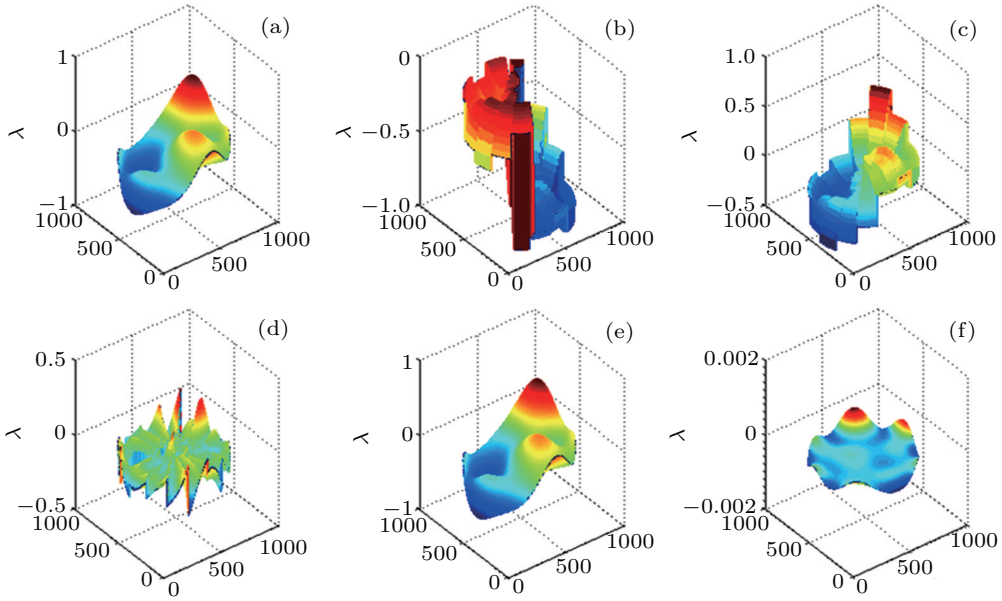


Fig. 3. (color online) Simulated wavefront and residual wavefront. (a) The incident wavefront (PV = 1.1560λ, RMS = 0.20λ). (b) The wrapped wavefront. (c) The discrete unwrapped wavefront. (d) The residual wavefront between the discrete unwrapped wavefront and the incident wavefront (PV = 0.4711λ, RMS = 0.0408λ). (e) The continuous reconstructed wavefront. (f) The residual wavefront between the reconstructed wavefront and the incident wavefront (PV = 0.0034λ, RMS = 0.0003λ).

The wavefront sensing frequency is important in an AO system. The wavefront sensing algorithm needs the intensity signals of the wavefront modulated with a series of modulation patterns. The number of the patterns means the time cost. So in order to increase the wavefront sensing frequency, the number of the MOW functions should be limited. We reconstruct the incident wavefront with the first 64 Walsh functions. The reconstruction result is shown in Fig. 4.

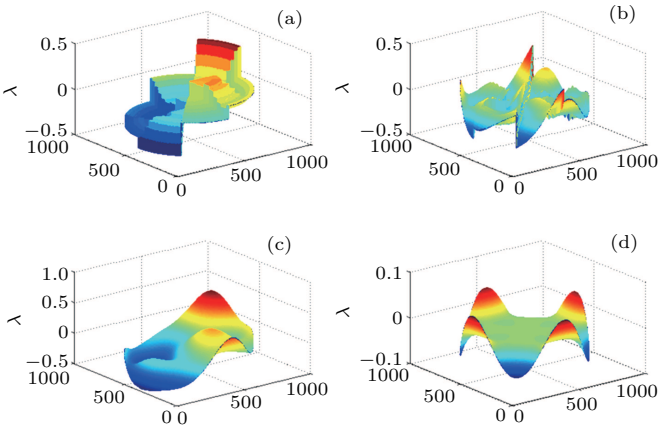


Fig. 4. (color online) Simulated wavefront and residual wavefront with the first 64 Walsh functions. (a) The discrete unwrapped wavefront. (b) The residual wavefront between the discrete unwrapped wavefront and the incident wavefront (PV = 0.7345λ, RMS = 0.0679λ). (c) The continuous reconstructed wavefront. (d) The residual wavefront between the reconstructed wavefront and the incident wavefront (PV = 0.1174λ, RMS = 0.0125λ).

Compared with the wavefront reconstructed with the first 256 Walsh functions, the wavefront reconstructed with the first 64 Walsh functions has a large residual. So the number of the Walsh functions used has a great impact on the reconstruction precision. Besides, some special Zernike orders cannot be reconstructed with the first 64 Walsh functions, such as the 13^{th} and 24^{th} orders. The wavefront generated with the first 35 Zernike polynomials cannot be reconstructed accurately with the first 64 Walsh functions.

The wavefront sensing algorithm can work well over different shapes. In fact, it can work well with different shapes of the pupil under the condition that the pupil can be divided into $2n$ (the index n can be any integer) units and the square of each unit is equal. We make a simulation to illustrate it. Figure 5 shows the wavefront reconstruction based on a rectangular pupil. The wavefront is generated randomly with the first 15 Legendre polynomials. We generate the transformation matrix from the discrete wavefront to a continuous one based on the Legendre polynomials. The residual error can reach a small value too.

Meanwhile, we reconstruct the wavefront with the stochastic parallel gradient descent (SPGD) algorithm. Firstly, we can detect the light intensities, I, of the light beam under different modulation patterns. Then in the parallel stochastic optimization, we assume that the initial values of the coefficients of the first 256 MOW functions are zeros. Next a two-side random ensemble small perturbation $\pm\delta c_j$ is simultane-

ously applied in parallel to all the coefficients of the MOW functions. The light intensities, I_+ and I_-, under different modulation patterns can be acquired. Then we can obtain the residual between I and I_+ or I_-, which is shown as follows:

$$\delta I_+ = I_+ - I, \quad \delta I_+ = I_+ - I. \tag{24}$$

We calculate the RMS, $I_{\mathrm{rms}+}$ and $I_{\mathrm{rms}-}$, of δI_+ and δ_-. The changed quality metric variation is shown as

$$\delta J = I_{\mathrm{rms}+} - I_{\mathrm{rms}-}. \tag{25}$$

Next we can obtain the SPGD algorithm for wavefront reconstruction as

$$c_j^{k+1} = c_j^k - \gamma \delta c_j \delta J, \tag{26}$$

where γ is a learning-rate parameter and c_j^k is the coefficients of the MOW functions of the k-th iteration. The reconstruction result is shown in Fig. 6.

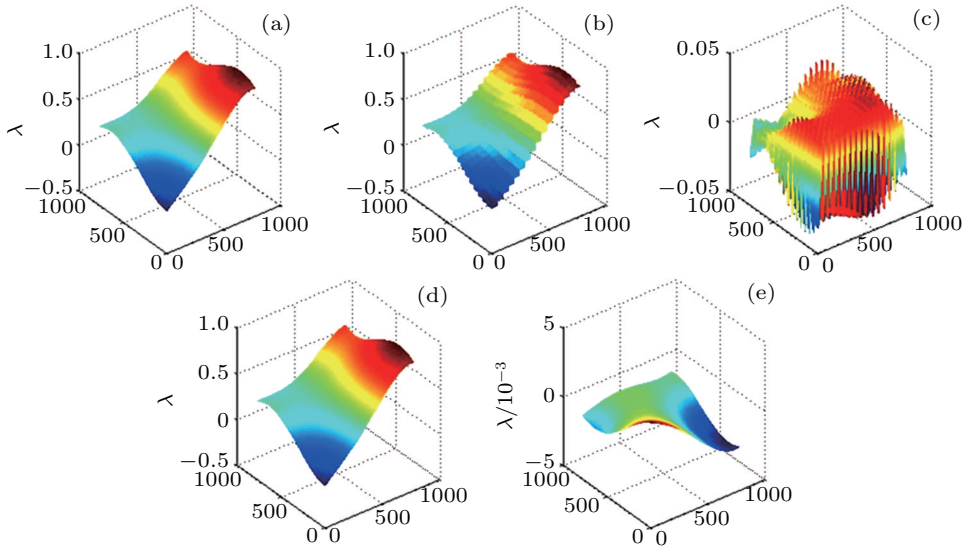


Fig. 5. (color online) Simulated wavefront and residual wavefront. (a) The incident wavefront (PV = 0.10037λ, RMS = 0.2251λ). (b) The discrete unwrapped wavefront. (c) The residual wavefront between the unwrapped wavefront and the incident wavefront (PV = 0.0842λ, RMS = 0.0143λ). (d) The continuous reconstructed wavefront. (e) The residual wavefront between the transformed wavefront and the incident wavefront (PV = 0.0047λ, RMS = 0.00089λ).

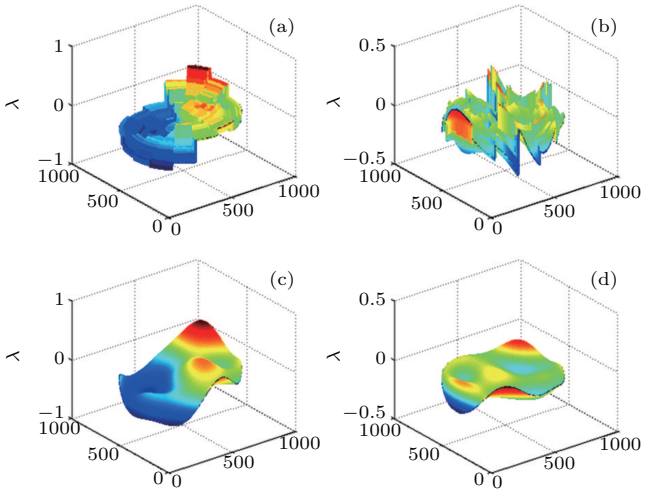


Fig. 6. (color online) Wavefront reconstructed with the SPGD algorithm. (a) The discrete unwrapped wavefront. (b) The residual wavefront between the discrete unwrapped wavefront and the incident wavefront; PV = 0.6255λ, RMS = 0.0583λ. (c) The continuous reconstructed wavefront. (d) The residual wavefront between the reconstructed wavefront and the incident wavefront; PV = 0.2912λ, RMS = 0.02λ.

As shown in Fig. 6, we can see that the wavefront reconstructed with the SPGD algorithm is similar to the incident wavefront. But the residual wavefront is larger than that reconstructed with the algorithm proposed in this paper. Meanwhile, we also compare the wavefront reconstruction time of the two methods. The algorithm proposed in the paper needs about 2.699 s and the SPGD algorithm needs about 67.921 s. It shows that the proposed algorithm has a higher speed compared with the SPGD algorithm. So it is demonstrated that the algorithm proposed in the paper has higher accuracy and speed.

5. Conclusion and perspectives

Benefitting from the high sensing speed and sensitivity of a single detector, sufficient signals can be acquired for wavefront sensing in an adaptive optics system. It provides a hardware foundation for the wavefront sensing method based on binary aberration modes applied in a real-time AO system. However, the coefficients of the MOW functions cannot be acquired with enough speed and accuracy by the iterative algorithm or optimization strategy. It restricts the use of the wavefront sensing method in adaptive optics.

In this paper, a new algorithm which can provide an analytical solution for the wavefront sensing method based on binary aberration modes is proposed. New modulation patterns are produced to build detailed and strict relationships.

The new modulation patterns can help to acquire the coefficients of the Walsh functions. A total of $3N-3$ intensity modulation patterns are generated for the wavefront reconstruction with N binary aberration modes. An analytical solution can be acquired by solving the equations and an accurate wavefront can be reconstructed. It provides a strong support for the wavefront sensing method, showing its great potentiality in adaptive optics.

As the algorithm can realize the reconstruction of the wavefront phase accurately, the wavefront sensing method could also be used in optical testing. A higher accuracy and a larger dynamic range can be achieved with more modulation modes. Besides, the method can sense a phase stage. So it may have a potential application in the reconstruction of the wavefront containing step jumps.

The algorithm acquires an analytical solution by adding new modulation patterns, which would require a relatively long time to achieve one measurement. This produces a limitation for its applications in a real-time AO system. It makes the wavefront sensing frequency of the method lower compared with that of the traditional method, such as the Shack–Hartmann wavefront sensing method. However, the frequency can be improved by compressing the number of modulation patterns. According to the Fourier diffraction theory, the sign of wavefront phase φ cannot be determined with the wavefront sensing method. Corresponding methods on how to determine the sign of the wavefront are necessary for the wavefront sensing method showing its potentiality in adaptive optics systems. The wavefront sensing algorithm still has some open questions. Further study is required to complete it.

References

[1] Robert K Tyson 2011 *Principles of Adaptive Optics* (3rd Edn.) (London: CRC Press) p. 111

[2] Hardy J W 1978 *Proc. IEEE* **66** 651

[3] Wang F L 2010 *Appl. Opt.* **49** G60

[4] He B, Hu L F, Li D Y, Xu H Y, Zhang X Y, Wang S X, Wang Y K, Yang C L, Cao Z L, Mu Q Q, Lu X H and Xuan L 2016 *Chin. Phys. B* **25** 094214

[5] Liang J, Grimm B, Goelz S, and Bille J 1994 *J. Opt. Soc. Am. A* **11** 1949

[6] Roddier F 1988 *Appl. Opt.* **27** 1223

[7] Gonsalves R A and Chidlaw R 1979 *Proc. SPIE* 0207 *Applications of Digital Image Processing III* August 27, 1979, San Diego, America, p. 32

[8] Booth M J 2006 *Opt. Express* **14** 1339

[9] Song H, Fraanje R, Schitter G, Kroese H, Vdovin G and Verhaegen M 2010 *Opt. Express* **18** 24070

[10] Wang F L 2009 *Appl. Opt.* **48** 2865

[11] Wang S, Yang P, Ao M W, Dong L and Xu B 2014 *Appl. Opt.* **53** 8342

[12] Qiao N S, Cai X H and Yao C M 2009 *Chin. Phys. B* **18** 4881

[13] Wang S, Yang P, Dong L, Xu B and Ao M W 2014 *Proc. of SPIE XX International Symposium on High-Power Laser Systems and Applications* August **25**, 2014, Chengdu, China, 9255 92553C-1

[14] Noll R J 1976 *J. Opt. Soc. Am.* **66** 207